applied optics

Large-aperture space optical system testing based on the scanning Hartmann

Haisong Wei,[1,2,*] Feng Yan,[1] Xindong Chen,[1] Hao Zhang,[1,2] Qiang Cheng,[1] Donglin Xue,[1] Xuefeng Zeng,[1] and Xuejun Zhang[1]

[1]Key Laboratory of Optical System Advanced Manufacturing Technology, Changchun Institute of Optics, Fine Mechanics and Physics, Chinese Academy of Sciences, Changchun, Jilin 130033, China
[2]University of Chinese Academy of Sciences, Beijing 100049, China
*Corresponding author: lwweihaisong@126.com

Received 1 November 2016; revised 2 February 2017; accepted 6 February 2017; posted 8 February 2017 (Doc. ID 279945); published 3 March 2017

Based on the Hartmann testing principle, this paper proposes a novel image quality testing technology which applies to a large-aperture space optical system. Compared with the traditional testing method through a large-aperture collimator, the scanning Hartmann testing technology has great advantages due to its simple structure, low cost, and ability to perform wavefront measurement of an optical system. The basic testing principle of the scanning Hartmann testing technology, data processing method, and simulation process are presented in this paper. Certain simulation results are also given to verify the feasibility of this technology. Furthermore, a measuring system is developed to conduct a wavefront measurement experiment for a 200 mm aperture optical system. The small deviation (6.3%) of root mean square (RMS) between experimental results and interferometric results indicates that the testing system can measure low-order aberration correctly, which means that the scanning Hartmann testing technology has the ability to test the imaging quality of a large-aperture space optical system.

OCIS codes: (220.4840) Testing; (120.3930) Metrological instrumentation; (120.4820) Optical systems; (080.0080) Geometric optics; (080.1010) Aberrations (global).

https://doi.org/10.1364/AO.56.002078

1. INTRODUCTION

The aperture of a space optical system has been increased for bigger field, higher resolution, and wider coverage of the space telescope. Evaluation of image quality of the optical system is essential before the telescope is launched into space. However, the wavefront aberration cannot be measured with interferometers after the focal plane of the optical system has been adjusted well. Currently, a collimated beam provided by a large collimator is always applied to pass through the optical system and focus on the sensor [1]. The detected spot's shape is recorded and analyzed to evaluate the performance of the system based on modulation transfer function (MTF). For instance, the Large Optical Test and Integration Site at Lockheed Martin Space Systems Company in Sunnyvale, California was designed and constructed in order to allow advanced optical testing for systems up to a maximum aperture of 6.5 m [2–4]. In this method, the aperture of the collimators are required to be the same with the optical system and the focal lengths are 3–5 times of the corresponding system, which results in a high and rising cost for the fabrication of these matched collimators. Thus, the replaced method with simpleness and high efficiency to perform image quality evaluation for a large-aperture space optical system is quite desired. The well-known James Webb Space Telescope (JWST) has a 6.6 m primary mirror aperture diameter. The JWST is tested at NASA's Johnson Space Center in the cryogenic vacuum chamber for alignment and optical performance. Nevertheless, the cryogenic optical test tower of the telescope is also extremely complex and expensive [5–8].

In order to solve the difficulty of testing a large-aperture optical system, a novel testing method based on the scanning Hartmann testing (SHT) principle is proposed in this paper. SHT uses a small collimator instead of a large and expensive collimator, and reduces the testing cost greatly. Furthermore, SHT can directly measure the optical system's wavefront slope and retrieve wavefront deformations by a wavefront reconstructed algorithm. Compared with the conventional testing way, which takes MTF as an evaluation index [9,10], SHT can measure wavefront aberration and characterize the variations that occur in an optical system. Therefore, SHT technology has a great potential in solving the testing problem of large-aperture space optical systems.

2. DESCRIPTION AND PRINCIPLE OF THE SCANNING HARTMANN TESTING

A. Basis Principle

The Hartmann testing is a simple and sensitive testing method to measure surface slopes and from those to retrieve the wavefront deformations [11]. The basic measured method is shown in Fig. 1, where the mirror under test is covered with a screen with holes (Hartmann screen). The spots are generated on the Hartmann plate when light passes through the holes. By examining the shift in position of the spots compared to that of an ideal mirror, the surface shape of the mirror can be determined. The principle of the scanning Hartmann testing is similar to the traditional Hartmann test, as in Fig. 2. More concretely, they both measure wavefront slope to retrieve wavefront deformations based on the geometric properties of light. In SHT, a small collimator scanning entrance pupil of the optical system corresponds to a Hartmann screen with holes used to shear beams. In the traditional Hartmann testing, the positions of a group of spots can be measured simultaneously on the Hartmann plate. However, in SHT, all spots are at the same position for an ideal optical system (performance of the ideal optical system is perfect) and around the ideal position for an actual optical system. Therefore, in order to avoid that these spots are too close to be resolved, a small collimator is adopted to scan the entrance pupil of the optical system and measure each sub-aperture spot's position one by one. The deviations between the spot positions and the ideal image point position are the wavefront slope's transverse aberrations of the homologous sub-apertures. Then the aberrations and wavefront map will be acquired through the wavefront reconstruction algorithm.

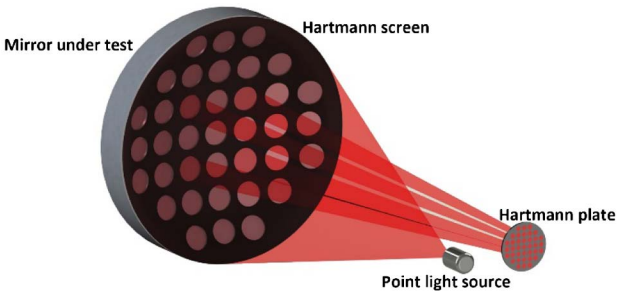

Fig. 1. Principle of classical Hartmann testing.

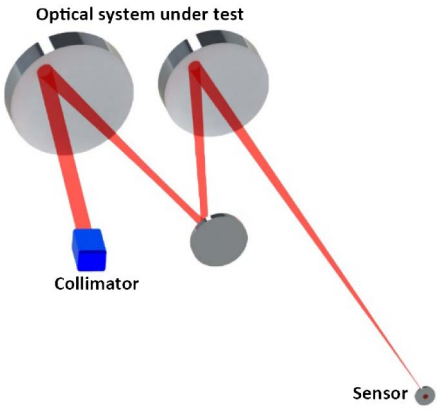

Fig. 2. Principle of scanning Hartmann testing.

B. Data Processing Method

1. Wavefront Reconstruction Algorithm

The wavefront reconstruction algorithm is based on the slope Zernike polynomial. The wavefront $\Phi(x, y)$ can be expressed as

$$\Phi(x, y) = \sum_{k=1}^{n} C_k Z_k(x, y). \tag{1}$$

The average slope of the sub-aperture wavefront in the X and Y directions is expressed as

$$\begin{cases} S_x = \frac{1}{A}\iint_A \dfrac{\partial \varphi(x, y)}{\partial x}\mathrm{d}x\mathrm{d}y \\ S_y = \frac{1}{A}\iint_A \dfrac{\partial \varphi(x, y)}{\partial y}\mathrm{d}x\mathrm{d}y \end{cases}. \tag{2}$$

Then, substitute formula (1) into formula (2). We can set up the relationship between average slopes and the slope Zernike modal coefficients:

$$\begin{bmatrix} \frac{\partial Z_{11}(x,y)}{\partial x} & \frac{\partial Z_{12}(x,y)}{\partial x} & \cdots & \frac{\partial Z_{1n}(x,y)}{\partial x} \\ \vdots & \vdots & \vdots & \vdots \\ \frac{\partial Z_{N1}(x,y)}{\partial x} & \frac{\partial Z_{N2}(x,y)}{\partial x} & \cdots & \frac{\partial Z_{Nn}(x,y)}{\partial x} \\ \frac{\partial Z_{11}(x,y)}{\partial y} & \frac{\partial Z_{12}(x,y)}{\partial y} & \cdots & \frac{\partial Z_{1n}(x,y)}{\partial y} \\ \vdots & \vdots & \vdots & \vdots \\ \frac{\partial Z_{N1}(x,y)}{\partial y} & \frac{\partial Z_{N2}(x,y)}{\partial y} & \cdots & \frac{\partial Z_{Nn}(x,y)}{\partial y} \end{bmatrix} \cdot \begin{bmatrix} C_1 \\ C_2 \\ \vdots \\ C_n \end{bmatrix} = \begin{bmatrix} S_{x1} \\ \vdots \\ S_{xN} \\ S_{y1} \\ \vdots \\ S_{yN} \end{bmatrix}. \tag{3}$$

The formula is simplified as

$$ZC = S. \tag{4}$$

Use the least-square method to solve the equations, namely,

$$C = (Z^T Z)^{-1} Z^T S. \tag{5}$$

After matrix C is brought into Eq. (1), the wavefront deformation can be calculated.

2. Effect of Positional Error of the Ideal Image Point

Based on the theory of geometrical aberration, the relation between the wavefront slope's transverse aberrations and the wavefront deformations is described as

$$\begin{cases} \mathrm{TA}_x = -\dfrac{L_{\mathrm{EP}}}{r_{\mathrm{EP}}} \cdot \dfrac{\partial W(x, y)}{\partial x} \\ \mathrm{TA}_y = -\dfrac{L_{\mathrm{EP}}}{r_{\mathrm{EP}}} \cdot \dfrac{\partial W(x, y)}{\partial y} \end{cases}, \tag{6}$$

where TA_x is the wavefront slope's transverse aberration in the x direction, TA_y is the wavefront slope's transverse aberration in the y direction, L_{EP} is the exit pupil distance of the optical system, and r_{EP} is the exit pupil semi-diameter. $W(x, y)$ is the corresponded sub-aperture's wavefront.

TA is the locational difference between the real spot and ideal image point. But the locational error of the ideal image point does not affect the reconstructed result of wavefront deformations. Assuming that the coordinate of the ideal image point is (x_0, y_0), the expressions (6) can be rewritten as

$$\begin{cases} \mathrm{TA}_x = (x - x_0) = -\dfrac{L_{\mathrm{EP}}}{r_{\mathrm{EP}}} \cdot \dfrac{\partial W(x,y)}{\partial x} \\ \mathrm{TA}_y = (y - y_0) = -\dfrac{L_{\mathrm{EP}}}{r_{\mathrm{EP}}} \cdot \dfrac{\partial W(x,y)}{\partial y} \end{cases}. \tag{7}$$

The expressions can be also rewritten through integration:

$$\begin{cases} W_x = -\int k(x - x_0)\mathrm{d}x = -\int kx\mathrm{d}x + kx_0 x \\ W_y = -\int k(y - y_0)\mathrm{d}y = -\int ky\mathrm{d}y + ky_0 y \end{cases}. \tag{8}$$

As the expressions (8) indicated, the coordinate (x_0, y_0) of the ideal image point manifests as the tilt term after integration. The reconstructed wavefront error introduced by this tilt displays the global tilt since all sub-aperture wavefronts have the same tilt term. However, what we are concerned with mostly in space optical system testing is the primary aberration, such as spherical aberration, coma, and astigmatism. Tilt could be removed directly from reconstructed wavefront and it does not affect the testing results. Therefore, we can draw a conclusion that the relative positions among a group of spots are significant rather than the absolute position, and the locational error of the ideal image point does not affect the final testing results.

C. Simulation

1. Simulation Analysis and Parameter Optimization

In order to verify the feasibility of the SHT principle, the whole testing process will be simulated on a computer, including the accurate calculation of the center of mass for spots with different sub-apertures, reconstruction of low-frequency wavefront aberration, and the influence of external error on the testing results. These simulation results can be used to analyze the testing accuracy and optimize the parameters in the next step.

Zemax and MATLAB are used to simulate the SHT process [12]. MATLAB works as a main program to offer instructions, and Zemax works as a ray tracing arithmetic unit to give feedback. Mzdde is used to realize the data transmission between them. On the basis of ray tracing results, the wavefront aberration is calculated precisely and the wavefront map is displayed in MATLAB. The schematic diagram of simulated testing is shown in Fig. 3. Specific simulated processes are illustrated as follows: first, the point light source is located at the system object surface at infinity, which can be regarded as the incidence of the plane wave. Then the small diaphragm is placed on the system entrance pupil to cut light beams, and a spot will be generated on the image surface after ray tracing. The spot position is recorded and the spot centroid is calculated precisely. In order to improve calculation precision of the spots centroid, the window method, threshold method, and gray weighting method will be adopted [13,14]. The next step is to measure the positional deviation between the spots centroid and ideal image point and calculate the slope of the corresponding sub-aperture wavefront. All the wavefront slope data of the sub-apertures will be acquired after the scanning. Finally, the wavefront can be reconstructed by Zernike polynomial fitting in MATLAB [15,16].

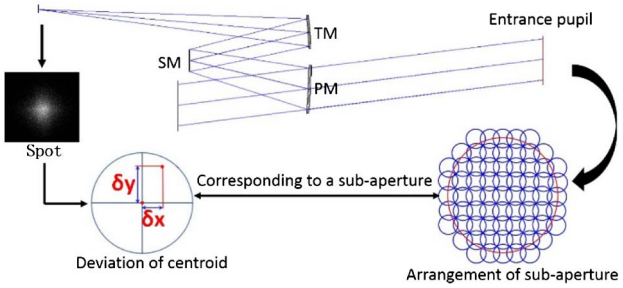

Fig. 3. Simulation of scanning Hartmann testing.

The optical system in Zemax is an off-axis three-mirror optical system with a focal length of 1999.47 mm, exit pupil distance of 2949.47 mm, entrance pupil caliber of 203.50 mm, and exit pupil caliber of 300.09 mm. Scanning Hartmann simulated testing is conducted for this system with 15 × 15, 31 × 31, and 63 × 63 sample densities and sub-aperture sizes of 20, 40, and 60 mm. The simulation results under different testing parameters are listed in Fig. 4 (the first 37 polynomials in Fringe Zernike). The simulated wavefront gets smooth and loses high-frequency error because the light of each sub-aperture passing through the optical system focuses to only one spot whose centroid position represents the mean result of low-, middle-, and high-frequency wavefronts of the corresponding sub-aperture. Figure 5 shows the spectrum of the actual wavefront and simulated wavefronts with different parameters. The middle- and high-frequency component of the simulated wavefronts are obviously reduced compared with that of the actual wavefront. With the sub-aperture size increasing, the middle- and high-frequency components decrease as well. Fortunately, the lack of middle- and high-frequency components does not

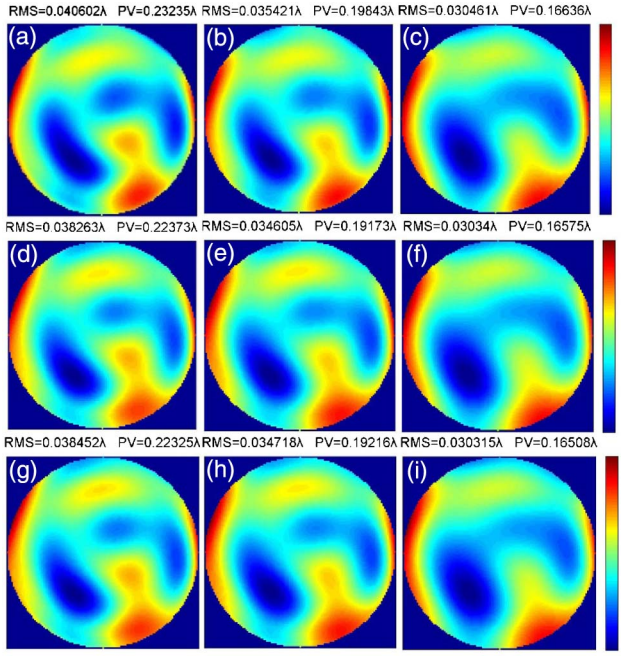

Fig. 4. Simulated wavefronts with different parameters: (a) 15 × 15 sampling density and 20 mm sub-aperture, (b) 15 × 15 sampling density and 40 mm sub-aperture, (c) 15 × 15 sampling density and 60 mm sub-aperture, (d) 31 × 31 sampling density and 20 mm sub-aperture, (e) 31 × 31 sampling density and 40 mm sub-aperture, (f) 31 × 31 sampling density and 60 mm sub-aperture, (g) 63 × 63 sampling density and 20 mm sub-aperture, (h) 63 × 63 sampling density and 40 mm sub-aperture, (i) 63 × 63 sampling density and 60 mm sub-aperture. The units of wavefront error are waves at a reference wavelength of 633 nm.

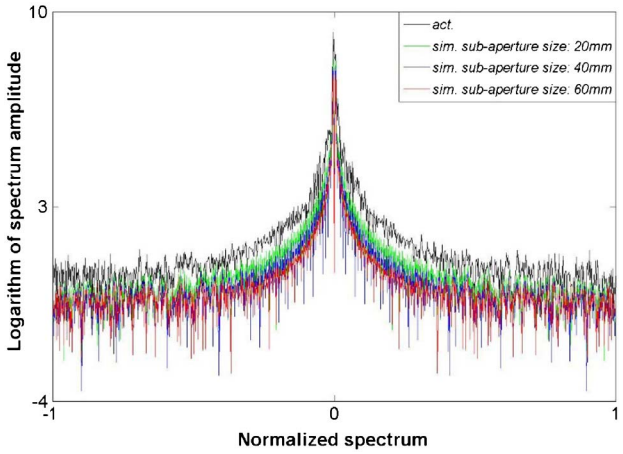

Fig. 5. Spatial frequency of simulated wavefronts.

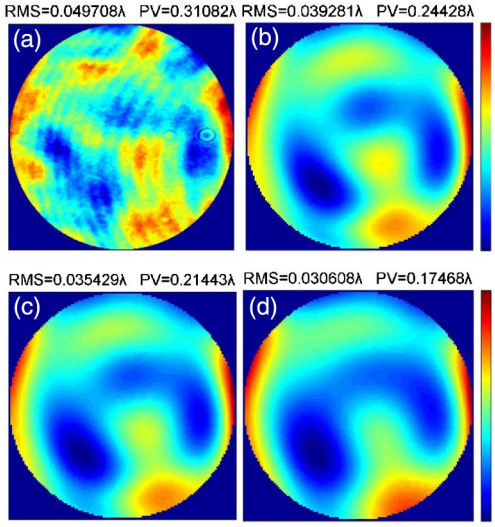

Fig. 6. (a) Wavefront map of optical system, (b) wavefront map with slope average filtering corresponding to 20 mm sub-aperture, (c) wavefront map with slope average filtering corresponding to 40 mm sub-aperture, and (d) wavefront map with slope average filtering corresponding to 60 mm sub-aperture.

affect availability in this testing stage, since we are concerned with low-frequency aberration influenced by variations of external stress and environmental temperature. Therefore, we do not put emphasis on the middle- and high-frequency aberration caused by the mirror manufacturing error.

The actual wavefront of the optical system will be processed with slope average filtering by comparing with the scanning Hartmann simulation results. The process of data processing can be summarized as follows. First, we figure up the partial derivatives of the wavefront in the X and Y directions to get the wavefront slope. Then we conduct average filtering for the wavefront slope and select different filtering templates for different sub-aperture sizes. The pixel number of the actual wavefront map is 1024 × 1024. Thus, when the sub-aperture diameter is 20 mm (1/10 of the system entrance pupil), the diameter of the wavefront filtering template is 102 pixels (1/10 of the wavefront map pixel number). Similarly, when the sub-aperture diameters are 40 and 60 mm, the diameters of the wavefront filtering template are 205 pixels and 307 pixels, respectively. At last, the wavefront slope with average filtering will be used for model method fitting to reconstruct wavefront aberration. As shown in Fig. 6, (a) is the actual wavefront map of the optical system, while (b), (c), and (d) are wavefront maps processed with slope average filtering corresponding to different sub-aperture sizes (the 37 polynomials in Fringe Zernike).

By comparing the SHT simulation results in Fig. 4 with the ideal wavefront processed with slope average filtering in Fig. 6, the difference of the root mean square (RMS) is about $\lambda/1000$ and the difference of the peak to valley is about $\lambda/50$ when sub-aperture sizes are identical. The high accuracy of the simulation results verifies the theoretical feasibility of SHT technology. The simulation results also indicate that SHT with a sample density of 15 × 15 and a sub-aperture size of 20 mm can accurately test low-order aberration of the system. Accordingly, in order to test more aberration information with high efficiency, the sample density 15 × 15 and the sub-aperture size of 20 mm are adopted in the next testing experiment.

2. Error Simulation Analysis

Error sources of SHT mainly come from the mechanical motion of two degrees of freedom scanning platform, including positioning error and pointing error, which respectively refer to the inaccurate positioning and inconformity pointing of the collimator in the scanning process. Influences of the collimator motion error on testing results will be analyzed by simulations so as to lay the foundation for follow-up testing experiments and engineering applications.

Eight types of motion errors are introduced in the process of simulations, as in Table 1. The sub-aperture size is 40 mm and the sample density is 127 × 127, and the wavefront reconstruction algorithm is the modal method based on the Zernike polynomial (the first 37 polynomials of Fringe Zernike). Simulated wavefronts are shown in Fig. 7.

As shown in Fig. 7, when the positioning error of the collimator exists, the simulated wavefront hardly varies no matter if this error is random or linear. Moreover, our motional platform reaches the positioning accuracy requirement of 0.05 mm, thus the positioning error of the collimator has no effect on SHT. When the random pointing error or high-frequency pointing error with 1 arcsec amplitude is introduced, the small variation of the simulated wavefront proves that the random pointing error and frequency pointing error have little influence

Table 1. Motion Errors of the Collimator in Simulation

	Positioning Error (mm)	Pointing Error (arcsec)
Random	Amplitude of ±0.05	Amplitude of ±1
High frequency		$\Delta\theta_x = \cos(20\pi x), x \in [-1, 1]$
Linear	$z_x = 0.05x, x \in [-1, 1]$	$\Delta\theta_x = x, x \in [-1, 1]$ $\Delta\theta_x = 0.1x, x \in [-1, 1]$
Low frequency		$\Delta\theta_x = \cos(\pi x), x \in [-1, 1]$ $\Delta\theta_x = 0.1\cos(\pi x), x \in [-1, 1]$

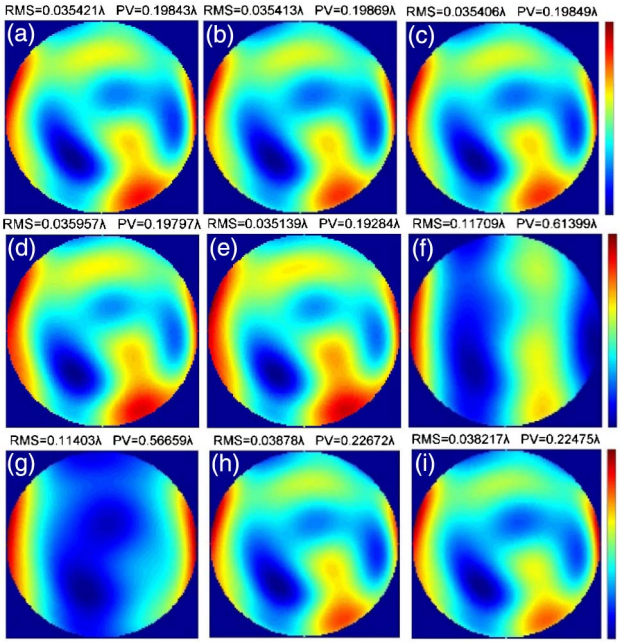

Fig. 7. Simulated wavefronts with different motion errors: (a) no motion error, (b) random positioning error, (c) linear positioning error, (d) random pointing error, (e) high-frequency pointing error, (f) low-frequency pointing error with amplitude of 1 arcsec, (g) linear pointing error with amplitude of 1 arcsec, (h) low-frequency pointing error with amplitude of 0.1 arcsec, (i) linear pointing error with amplitude of 0.1 arcsec.

on low-frequency testing results. The simulated wavefront changes significantly when the pointing error is a linear error or a low-frequency error with 1 arcsec amplitude, and wavefront deformation caused by those errors completely covers the wavefront shape of the system so that low-frequency aberration cannot be decoupled from the testing results. When the amplitude of the linear or low-frequency error drops to 0.1 arcsec, the RMS value changes by 9.3% and the wavefront shape is generally similar. Therefore, the low-frequency component of the pointing errors which belong to the system error should be calibrated accurately and rectified within 0.1 arcsec based on the calibration results. The residual high-frequency errors which belong to random errors do not influence the low-frequency testing results of the optical system.

3. EXPERIMENT

A. Experimental Design

An experiment was designed and conducted to test an optical system's wavefront aberration, and the result would be contrasted with the interferometric results. The experiment aimed to demonstrate the theoretical feasibility of the SHT, so the error source should be got rid of as soon as possible. In order to avoid the pointing error of the collimator, we adopted the alternative operation manner that a collimated beam emitted by a large collimator was sheared to a small diameter beam by the mask with a hole in the center instead of single small collimator scanning. With the mask's continuous movement along the given trajectory, many small diameter collimated beams with different positions and same pointing were successively generated.

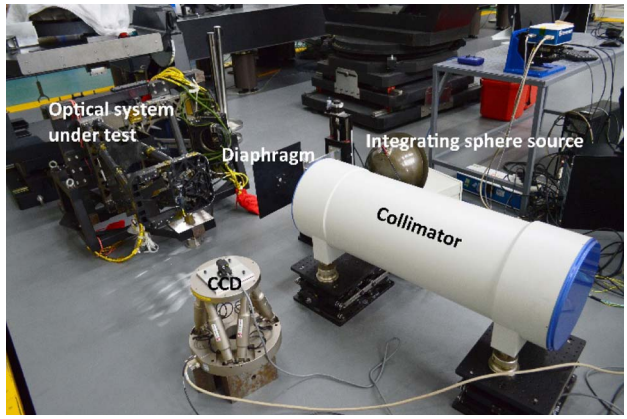

Fig. 8. Optical layout of the testing system.

The optical layout of the testing system for this experiment is shown in Fig. 8. The optical system to be tested was an off-axis three-mirror optical system with a focal length of 1999.47 mm and clear aperture of 203.50 mm at a single field. In the object space of the system, a large collimator with wavefront RMS of $\lambda/50$ and integrating sphere source were set up to generate collimated incident light. The $X-Y$ translation stage was put between the large collimator and the optical system. On the focal surface of the system, the charge-coupled device (CCD) with 1600 × 1200 pixels and 4.4 μm pixel size was mounted on a high-accuracy six-axis motion platform to perform precise focusing. Finally, the whole experiment was shaded with a black hood to eliminate the disturbance of stray light. During the testing, the computer automatically controlled the mask moving according to beforehand trajectory and residing in the sampling position while it gathered the spot image on the CCD and calculated the spots centroid. Wavefront aberration of the optical system will be fitted and reconstructed after this testing.

B. Experiment Results

On the basis of the simulation analysis mentioned above, the sub-aperture size of 20 mm and the sample density of 15 × 15 are adopted. All spots of the sub-aperture on the focal surface are shown in Fig. 9. The wavefront map of the testing results in Fig. 10(a) is similar with that of the interferometric results processed with slope average filtering in Fig. 10(b). The RMS variation of 6.3% indicates that the SHT has the ability to test the low-order aberration of the optical system.

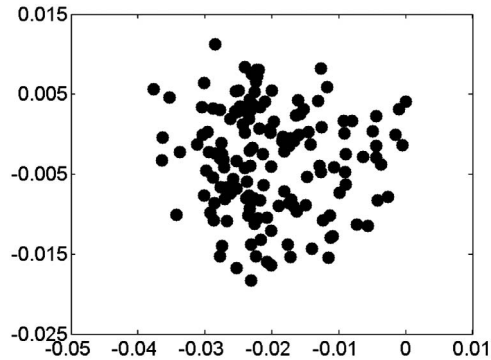

Fig. 9. All of the spots on CCD (mm).

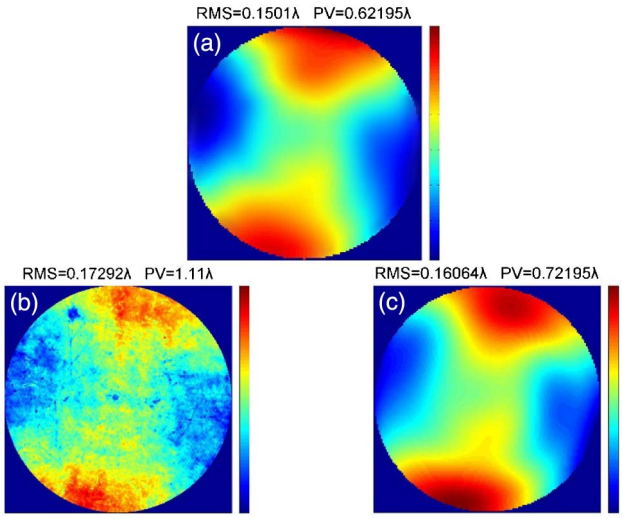

Fig. 10. (a) The wavefront map by SHT, (b) the wavefront map in interferometer, and (c) the wavefront map with slope average filtering in interferometer.

C. Error Analysis

There are main two reasons for the testing error:

(a) In the SHT experiment, the source of the collimator was an integrating sphere in which three heavy heat xenon lamps were fixed so that the large temperature gradient was generated and intensified airflow disturbance in the airtight experiment surrounding. Its influences became larger as testing time went on. However, this error influence could be almost reduced by the use of a cold light source.

(b) The spots on the focus plane did not have the same brightness and some spots were conspicuously darker than the others during the experiment testing process. The reason was that the mirror coating of the optical system had suffered some damage resulting in uneven distribution of mirror reflectivity, which had no effect on the interferometric results but did have great effect on SHT [17]. The uneven distribution of mirror reflectivity means that the weight of each ray was different in spots centroid calculation. The inaccurate centroid position would influence the testing results.

4. CONCLUSION

A novel image quality testing technology which applies to a large-aperture space optical system is proposed in this paper. Comparing with the traditional testing method, which measures MTF by the use of a large-aperture collimator, the SHT has great advantages due to its simple structure, low cost, and ability to realize wavefront measurement which can vividly embody the characteristic of the optical system. This paper verifies the feasibility of this testing technology in two respects. First, simulation results manifest that the RMS deviation of the simulated wavefront is about $\lambda/1000$ compared with the ideal wavefront, which verifies theoretical feasibility of SHT. Second, the RMS deviation of 6.3% between the experimental results and the interferometric results for a 200 mm aperture optical system indicates that this testing system can correctly measure low-order aberration, and also demonstrates that this scanning Hartmann testing technology has the ability to test image quality of a large-aperture optical system.

Funding. National Natural Science Foundation of China (NSFC) (61210015); National Youth Foundation of China (61605202).

REFERENCES

1. D. W. Kim, W. Cai, and J. H. Burge, "Use of thermal sieve to allow optical testing of cryogenic optical systems," Opt. Express **20**, 12378–12392 (2012).
2. R. M. Bell, G. C. Robins, C. Eugeni, G. Cuzner, S. B. Hutchison, S. H. Baily, B. Ceurden, J. Hagen, K. Kenagy, H. M. Martin, M. Tuell, M. Ward, and S. C. West, "LOTIS at completion of collimator integration," Proc. SPIE **7017**, 70170D (2008).
3. S. B. Hutchison, A. Cochrane, S. McCord, and R. Bell, "Updated status and capabilities for the LOTIS 6.5 m collimator," Proc. SPIE **7106**, 710618 (2008).
4. S. C. West, S. H. Bailey, J. H. Burge, B. Cuerden, J. Hagen, H. M. Martin, and M. T. Tuell, "Wavefront control of the large optics test and integration site (LOTIS) 6.5 m collimator," Appl. Opt. **49**, 3522–3537 (2010).
5. L. D. Feinberg, J. G. Hagopian, and C. Diaz, "New approach to cryogenic optical testing the JWST," Proc. SPIE **6265**, 62650P (2006).
6. C. Atkinson, J. Arenberg, G. Matthews, M. Waldman, A. Wertheimer, T. Whitman, and J. Oschmann, "Architecting a revised optical test approach for JWST," Proc. SPIE **7010**, 70100Q (2008).
7. L. D. Feinberg, A. Barto, M. Waldman, and T. Whitman, "James Webb Space Telescope system cryogenic optical test plans," Proc. SPIE **8150**, 815007 (2011).
8. J. S. Knight, L. Feinberg, J. Howard, D. S. Acton, T. L. Whitman, and K. Smith, "Hartmann test for the James Webb Space Telescope," Proc. SPIE **9904**, 99040C (2016).
9. R. Fu, N. Wu, X. Zhang, Y. Qiu, and B. Chang, "The design of MTF test system based on point light source," Proc. SPIE **8126**, 81260Q (2011).
10. J. Xin, "Investigation on the MTF for the large-aperture long focal length TDICCD camera," Proc. SPIE **8416**, 84161L (2012).
11. D. Malacara-Hernández and D. Malacara-Doblado, "What is a Hartmann test?" Appl. Opt. **54**, 2296–2301 (2015).
12. F. Yan and X. Zhang, "Optimization of an off-axis three-mirror anastigmatic system with wavefront coding technology based on MTF invariance," Opt. Express **17**, 16809–16819 (2009).
13. X. Yin, X. Li, L. Zhao, and Z. Fang, "Adaptive thresholding and dynamic windowing method for automatic centroid detection of digital Shack–Hartmann wavefront sensor," Appl. Opt. **48**, 6088–6098 (2009).
14. S.-H. Baik, S.-K. Park, C.-J. Kim, Y.-S. Seo, and Y.-J. Kang, "New centroid detection algorithm for the Shack–Hartmann wavefront sensor," Proc. SPIE **4926**, 251–260 (2002).
15. J. Yu, F. Fang, and Z. Qiu, "Aberrations measurement of freeform spectacle lenses based on Hartmann wavefront technology," Appl. Opt. **54**, 986–994 (2015).
16. H.-S. Yang, Y.-W. Lee, J.-B. Song, and I.-W. Lee, "Null Hartmann test for the fabrication of large aspheric surfaces," Opt. Express **13**, 1839–1847 (2005).
17. X. Ma, J. Mu, C. Rao, J. Yang, X. Rao, and Y. Tian, "Extension of the modal wave-front reconstruction algorithm to non-uniform illumination," Opt. Express **22**, 15589–15598 (2014).